EARTH OBSERVATION AND GEOMATICS ENGINEERING
website: https://eoge.ut.ac.ir

Mineral prospectivity mapping of porphyry Cu deposit using VIKOR method

Mahyadin Mohammadpour[1] , Abbas Bahroudi [1]*, Maysam Abedi[1]

[1] Department of Mining Engineering, University of Tehran, Tehran, Iran

Article history:
Received: 19 March 2020, Received in revised form: 20 August 2020, Accepted: 28 August 2020

ABSTRACT

Naysian *Porphyry* Cu District (NPCD) is situated northeast of Isfahan, in the center of Iran along the Urumia-Dokhtar Magmatic Assemblage (UDMA) belt. Mineral Potential Mapping (MPM) is an important issue in mining to reduce the exploration costs by proposing a layout of drilling over the most favorable regions in association with an ore-bearing target. MPM can be defined as a multi-criterion decision-making (MCDM) problem. Out of many MCDM methods, the VIKOR is based on a compromise solution which evaluates issues with inappropriate and incompatible criteria. In this study, seven geospatial indicators related to the NPCD were extracted from geological, geochemical, and geophysical criteria. According to the conceptual model of a porphyry copper mineralization system, the highest weight was allocated to the geochemical criterion with a value of 0.499 and the sublayer of the copper concentration map (0.425). In addition, the lowest weight was allocated to the geophysical criterion (0.113). Two variants of the VIKOR method that are the conventional (C-VIKOR) and the adjusted (A-VIKOR) ones were examined in this study, and their outputs were compared with the index overlay (IO) method as a popular approach in MPM. Taking a threshold value of 0.6 into account for final synthesized indicators, the mineral favorability areas highlighted by the IO, A-VIKOR, and C-VIKOR methods have occupied 49.5, 15.8, and 18.7 hectares, respectively. It is worth pointing out that the MPM derived from the A-VIKOR method has superiority over the outputs of the IO and C-VIKOR methods by introducing the lowest favorable area and 92% matching of high-grade boreholes with the proposed areas. Comparing the mean grade of copper obtained from boreholes drilled in the area and the values of MPM, a significant correlation between boreholes and prospectivity map was also obtained.

KEYWORDS
C-VIKOR
A-VIKOR
Index Overlay
Porphyry Copper
Naysian District.

1. Introduction

One of the most important steps in the exploration of mineral deposits is to identify favorable areas in association with ore-bearing mineralization. In this regard, different geospatial information layers derived from geological, geochemical, geophysical, and so on, are collected over the study area, and then processed to synthesize different exploratory indicators. It is so-called "Mineral Potential Mapping (MPM)" which delimits a deposit or district scale prospecting region into several highly favorable areas. Therefore, MPM can be assumed as a multi-criteria decision-making (MCDM) problem, since it aims to produce predictive maps based on different exploratory criteria (Abedi et al., 2016; Abedi, Ali Torabi, et al., 2012; Abedi, Norouzi, & Fathianpour, 2012; Abedi & Norouzi, 2016; Najafi et al., 2014). The concept of MPM was first introduced by Cargill and Clark (1978), which was laid as a base for many studies, and later a large number of scholars have developed a wide range of models to integrate exploratory geospatial data sets (Cargill & Clark, 1978). These methods of MPM are often classified into three main groups that are knowledge-, data-driven, and hybrid.

Hidden spatial relations between known deposits and various evidential layers are sought through samples of

* Corresponding author
E-mail addresses: m_mohammadpour@ut.ac.ir (M. Mohammadpour); bahroudi@ut.ac.ir (A. Bahroudi); maysamabedi@ut.ac.ir (M. Abedi).
DOI: 10.22059/eoge.2020.305708.1083

training data points in the data-driven MPM methods. Therefore, these methods are usually employed in a well-explored area with known mineral occurrences (Bonham-Carter, 1994). Among various methods of this group, the main ones are weights of evidence (Porwal et al., 2001), artificial neural network (Oh & Lee, 2010; Porwal et al., 2003), support vector machine (SVM) (Abedi, Norouzi, & Bahroudi, 2012), and random forest (Emmanuel John M. Carranza & Laborte, 2015). In the knowledge-driven MPM method, the pieces of evidence are weighted and subsequently integrated based on experts' judgments. Hence, knowledge-driven MPM methods may lead to uncertainty in spatial data due to the bias weighting of each expert (Emmanuel John M. Carranza, 2009). These methods are index overlay (Billa et al., 2004), fuzzy logic (Abedi et al., 2012b; Abedi et al 2015, Najafi et al., 2014), fuzzy-AHP (Abedi et al., 2013), and wildcat mapping (Emmanuel John M. Carranza, 2010). Hybrid methods combine the experts' knowledge and the location of known mineral occurrences, known as data-knowledge-driven approaches (e.g., Carranza et al., 2008; Porwal et al., 2006; Yousefi and Carranza, 2015). Some data-driven methods use an experimental function and select the weights for the evidential features based on the expert judgment. Also, the method does not act based on the training data points (Emmanuel John M. Carranza, 2010; Luo & Dimitrakopoulos, 2003).

Out of many MCDM algorithms, the VIKOR outranking method has been successfully used as a knowledge-driven MPM (Abedi et al., 2016; Ghezelbash & Maghsoudi, 2018). Opricovic (1998), introduced the VIKOR method, which is based on a compromise solution by evaluating issues with inappropriate and incompatible criteria. When a decision-maker is unable to identify and express the superiority of an issue at the time it is started and designed, the VIKOR can be an appropriate tool for decision making (Opricovic & Tzeng, 2004). Of note is that the VIKOR method of compromise ranking determines a compromise solution, provides a maximum ''group utility'' for the ''majority'' and a minimum of an individual regret for the ''opponent''. When implementing a VIKOR method, a linear normalization is used to eliminate and scale the units of diverse criteria (Opricovic & Tzeng, 2004).

The main purpose of this study is to compare the performance of two variants of the VIKOR methods for synthesizing indicator layers. Two conventional (C-VIKOR) and adjusted (A-VIKOR) variants were used in MPM and their outputs were compared to the index overlay (IO) method as a popular MPM methodology. In order to assign weight to the evidential/indicator layers by the VIKOR method, it is first necessary for continuous maps to be broken down into different classes. One of the methods of anomaly separation from the background is the concentration-area (C-A) fractal method, which in addition to data frequency distribution, determines their spatial variability in computation with a high level of confidence (Cheng et al., 1994). A data set pertaining to the Naysian *Porphyry* Cu District (NPCD) in Iran is used in this study.

Naysian district is located about 73 km away from the northeast of Isfahan. This prospecting area is aligned along the UDMA (Alavi, 2004). Based on reconnaissance studies such as field survey, geophysics remote sensing, lithological and mineralogical studies, this district is known to be prone to porphyry copper and molybdenum reserves (Afshooni et al., 2013; Farmahini Farahani, 2008; Hatami, 2008; Tabatabaei, S.H., Asadi Haroni, 2006). Farmahini Farahani (2008) and Afzal et al. (2013) introduced the Naysian as a classic porphyry system and believed that the model of alteration and mineralization of this deposit was similar to the world-known models (Afzal, Harati, et al., 2013; Farmahini Farahani, 2008). Hatami (2008) introduced the processes affecting the formation of igneous rocks of Naysian ancient porphyry deposit, including three categories of separation crystallization, the effects of intense alteration activities on them, and the fragmentation and shear of igneous rocks. Based on geological and exploratory studies, this deposit has been divided into three eastern, central, and western parts. The studies show a better condition of the eastern and central parts of this deposit and more exploratory studies have been dedicated to these two parts (Afzal et al., 2010; Tabatabaei, S.H., Asadi Haroni, 2006). According to the studies carried out to explore the Naysian deposit, the definite copper reserve of this deposit is about 40 million tons with a grade of 0.053%, and it is about 120 million tons for Mo with a grade of 0.02%(Asadi Haroni, 2007).

In this study, seven geospatial evidence layers over the NPCD were extracted and separated into different populations using the C-A fractal model to assign an appropriate score and weight for each layer. Then, the final decision matrix is prepared based on the weights of the criteria and sub-criteria, and MPMs were generated through implementing two variants of the VIKOR and the IO methods, where the efficiency of each map was evaluated with drilling results as well.

2. Methodology

2.1. VIKOR method

The VIKOR method was first introduced by Opricovic (1998) as a powerful MCDM technique to efficiently rank multi-attribute problems with different criteria. Indeed, it ranks and selects from a set of alternatives in the presence of conflicting multi-criteria, by introducing a multi-criteria ranking index based upon a measure of "closeness" to an "ideal solution" (Opricovic, 1998; Opricovic & Tzeng, 2004). The formulation of the conventional "C-VIKOR" and the adjusted "A-VIKOR" variants are concisely presented as

follows,

Assume that $A_i(i = 1,2, \dots, n)$ and $C_j(j = 1,2, \dots, m)$ are a set of n alternatives and m criteria/attributes respectively. The C-VIKOR method can be described in a series of steps;

Step 1: Construct a decision matrix from the geospatial data sets by assigning a priority score $X = (x_{ij})_{n\times m}$ to each alternative i on each criterion j.

Step 2: Determine the weight (w_j) of all criteria (through Delphi method in this study) such that;

$$\sum_{j=1}^{m} w_j = 1, \quad j = 1,2, \dots, m. \tag{1}$$

Step 3: Obtain the normalized decision matrix (r_{ij}) to avoid scaling effects perturbing the result,

$$r_{ij} = x_{ij} / \left(\sum_{p=1}^{n} x_{pj}^2\right)^{0.5}, \quad i = 1,2, \dots, n \ \& \ j = 1,2, \dots, m \tag{2}$$

Step 4: Determine the best $f_j^+$and the worst f_j^- values of all criteria,

$$f_j^+ = \left(f_1^+, f_2^+, \dots, f_j^+, \dots, f_m^+\right) = \left\{\left(\max_i\{r_{ij}\} | j \in B\right), \left(\min_i\{r_{ij}\} | j \in C\right)\right\} \tag{3}$$

$$f_j^- = \left(f_1^-, f_2^-, \dots, f_j^-, \dots, f_m^-\right) = \left\{\left(\min_i\{r_{ij}\} | j \in B\right), \left(\max_i\{r_{ij}\} | j \in C\right)\right\} \tag{4}$$

where B and C correspond to the benefit and cost criteria, respectively (Tavana & Hatami-Marbini, 2011).

Step 5: Compute the values of $S_i$and R_i from the following equations. Development of the VIKOR method started from L_k-metric as (Opricovic & Tzeng, 2004),

$$L_{k,i} = \left(\sum_{j=1}^{m}\left[w_j\left(f_j^+ - r_{ij}\right)/\left(f_j^+ - f_j^-\right)\right]^k\right)^{1/k}, 1 \le k \le \infty \tag{5}$$

Here the values of $S_i$and R_i are calculated from Eq. (5),

$$S_i = L_{1,i} = \sum_{j=1}^{m} w_j\left(f_j^+ - r_{ij}\right)/\left(f_j^+ - f_j^-\right) \tag{6}$$

$$R_i = L_{\infty,i} = \max_j\left(w_j\left(f_j^+ - r_{ij}\right)/\left(f_j^+ - f_j^-\right)\right) \tag{7}$$

Step 6: Compute the values of Q_i for each alternative i from the following equation;

$$Q_i = v\left(\frac{S_i - S^-}{S^+ - S^-}\right) + (1 - v)\left(\frac{R_i - R^-}{R^+ - R^-}\right), \quad 0 \le v \le 1 \tag{8}$$

where

$$\begin{cases} S^+ = \max_i S_i, S^- = \min_i S_i \\ R^+ = \max_i R_i, R^- = \min_i R_i \end{cases}$$

and parameter v is introduced as a weight for the strategy of the majority of criteria "$\frac{S_i - S^-}{S^+ - S^-}$" and $(1 - v)$ is the weight of the individual regret "$\frac{R_i - R^-}{R^+ - R^-}$". The value of v lies in a range of $[0,1]$ and in most cases, it was chosen equal to $v = 0.5$ for a compromise solution (Abedi et al., 2016).

Step 7: Compute MPM values of M_i^{V-C} for synthesized data as,

$$M_i^{V-C} = \frac{Q^+ - Q_i}{Q^+ - Q^-} \tag{9}$$

where $Q^+ = \max_i Q_i$ and $Q^- = \min_i Q_i$. Higher values of M_i^{V-C} correspond to higher potential zones for ore occurrences in the region of interest.

To implement an A-VIKOR method proposed by Jahan et al. (2011), the values of $S_i$and R_i are calculated from the following equations to determine M_i^{V-A} while the other steps are similar to the C-VIKOR method (Jahan et al., 2011).

$$S_i = \sum_{j=1}^{m} w_j\left(1 - e^{\frac{|r_{ij} - f_j^+|}{f_j^- - f_j^+}}\right) \tag{10}$$

$$R_i = \max_j\left[w_j\left(1 - e^{\frac{|r_{ij} - f_j^+|}{f_j^- - f_j^+}}\right)\right] \tag{11}$$

2-2- A C-A fractal model

Many natural processes, especially those related to earth sciences, do not follow regular Euclidean geometry, so one must use another geometry to describe events in nature. Thus, for the first time in 1983, Mandelbrot introduced a geometry that could discuss the processes in nature and called it fractal geometry (Mandelbrot, 1983). For the first time, Cheng et al. (1994) used the Mitchel-Sulfurests Porphyry Cu-Au in British Columbia, Canada to separate geochemical anomalies and background from each other (Cheng et al., 1994). In general, the exploration data have multifractal behavior indicating the extent of changes in geological, tectonic, geochemical, geophysical, alteration, and subsequent enrichment and ore formation stages. By matching these features to field data and observations, the accuracy of multifractal modeling is well established (Afzal, Ahari, et al., 2013; M. Mohammadpour et al., 2019; Zuo et al., 2009). A C-A fractal method is based on the amount of space that each specific concentration occupies in the study area and is presented on the basis of a series of simple empirical equations (Cheng et al., 1994) .This empirical model states that the area A (ρ) follows an exponential relation by setting the values of ρ less than or equal to a predetermined threshold value υ:

$$A(\rho \le \vartheta) \infty \rho^{-\alpha} \tag{12}$$

Where A(ρ) is an area of higher concentration than the curve ρ, υ expresses a threshold and α is a fractal dimension (Cheng et al., 1994).

3. Geological Setting

The NPCD with an area of about 6 km^2 is located about 72 km away at the northeast of Isfahan. This deposit is tectonically located in the UDMA belt (Figure 1a) (Aghanabati, 2004; Stocklin, 1968), which is formed as a volcanic belt with a general northwest-southeast trend consisting of Eocene-Quaternary age volcanic and intrusive bodies (Berberian & Berberian, 1981). The UDMA zone is elongated in east-northeast of the Sanandaj-Sirjan zone and

west-southwest of the Central Iran zone (Aghanabati, 2004; Sabahi et al., 2019).

The NPCD system was previously studied in enormous researches (e.g. Afshooni et al., 2013; Afzal et al., 2010; Tabatabaei, S.H., Asadi Haroni, 2006). Concerning the petrological investigations, the volcanic rocks of this area are dacite, andesite, basaltic andesite, and basalt, and the intrusive rocks contain a combination of granodiorite and tonalite. In addition, magma content is of sub-alkaline and calco-alkaline types. The alteration processes are wide and severe on the NPCD. The main observable alterations, in the expansion order, are propylitic, phyllic, potassic, quartz–tourmaline, silica, and FeO zones (Zarnab Co., 2011).

Naysian area is tectonically active and dynamic. The presence of extended faults with a trend around N55E and their interactions with the perpendicular faults of the UDMA zone has been effective in emplacing the stocks in the zone and expanding the alteration processes in rock units. The general trend of magmatic dikes injected in this zone is along the NE-SW (Zarnab Co., 2011). The geological map in the 1:1000 scale for the studied zone is presented in Figure 1, which presents the rock type distributions.

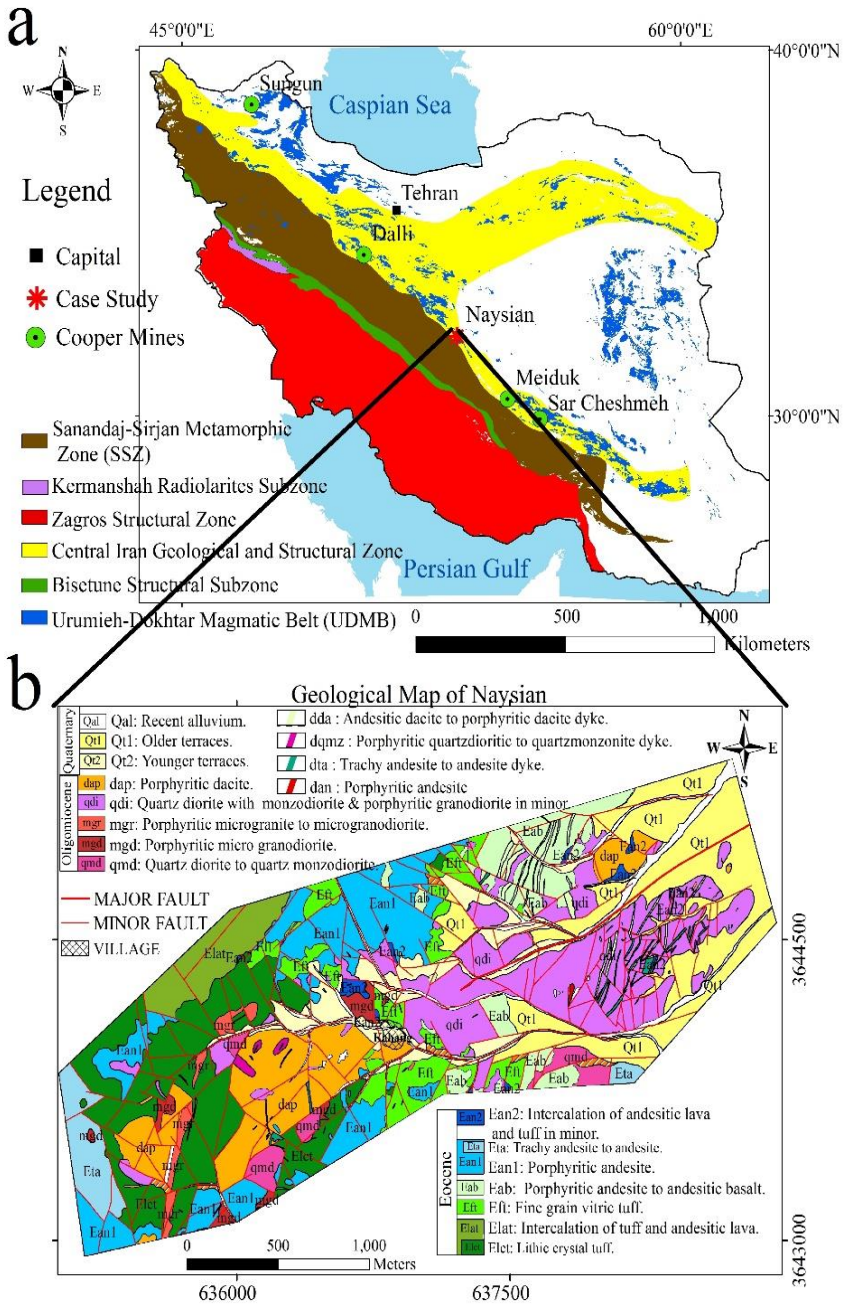

Figure 1. (a) The position of the Naysian Porphyry copper deposit in the Iranian structural geology divisions, b) Geological Map of the Naysian Porphyry Copper district with a scale of 1: 5000.

4. Exploratory Information System (EIS)

Information systems help organize, analyze, and convert raw data into useful information for the purpose of supporting and improving decision-making (Laudon &

Laudon, 2014). One of the examples designed to support decision-making in earth sciences, with which most earth scientists are familiar, is the Geographic Information System (GIS). An exploratory information system (EIS) is required to convert data into insight, and GIS technology is used to explore minerals. EIS is defined as a framework for; (1) collecting regular and systematic data, (2) defining target characteristics and criteria, (3) generating target proxies or exploratory layers, and finally (4) integrating target criteria (Yousefi et al., 2019). EIS can be quickly used to generate exploration targets using a variety of integration functions. As an efficient system, EIS has been used to integrate evidential geospatial layers in this paper.

4.1. Exploratory geospatial data sets

Data clearance has a significant impact on the type and quality of exploratory information related to the purpose of exploration. On a regional scale, for instance, existing data typically have a lower resolution, while overall data on a deposit scale has a higher resolution. Therefore, the methods of preparing exploratory data should be selected based on the scale of mineral exploration. Given the introduction of the studied area in section 3 and the area under study (6 km^2), the phase of exploratory studies is on a local scale, and it is expected that the map of the mineral potential of this stage determines the mineral prospectivity areas for detailed operations including litho-geochemistry, geoelectrical surveys and designing the layout of drilling.

Mineral exploration data are divided into five broad categories: (I) geology, (II) geochemical data, (III) geophysical data, (IV) remote sensing, and (V) drilling (Yousefi et al., 2019). In this paper, different types of exploratory data have been used according to the exploratory scale, which will be mentioned below. Naysian exploration district is lithologically composed of different rocks such as andesite, porphyry andesite, porphyry dacite, shear volcanic rocks, microdiorite, and quartz monzonite (Hatami, 2008; Hosseini, 2011). All rocks in the area have been altered partially to large extent by hydrothermal fluids and have been affected by phyllic, argillic, and propylitic alterations (Afshooni et al., 2013; Azadi et al., 2015). The main minerals include hematite, goethite, jarosite, malachite, and azurite belonging to the oxide zone, chalcopyrite, chalcocite, and covellite belonging to the supergene zone, and chalcopyrite, pyrite, and magnetite belonging to the hypogene zone. In NPCD, there are several main faults with two trends of NE-SW and NW-SE, and the ore-bearing mineralization in the region is almost controlled by these tectonic structures (Asadi Haroni, 2007). Due to the area of the exploratory district, the geological map at a scale of 1: 5000 was prepared by Zarnab Company as a field survey. Geological map information was used to prepare MPM.

One of the most effective methods for the exploration of metallic low-grade deposits, such as Cu, is the geochemical method, which was used here due to the good soil cover in the area and an exploration scale of 1: 5000. In this method, each sample has a greater radius impact than the litho-geochemical method, and it can be said that the soil-geochemical method is a suitable method in this scale and stage of exploration. Based on the geological map and mineralization process in the area, a 50 × 25 m rectangular grid was designed for soil sampling so that the rectangular length was in the direction of mineralization. 2564 soil geochemical samples were collected in the area and analyzed by the ICP-OES method (Zarnab. Co, 2011). After chemical analysis of the specimens, the results were subjected to preprocessing and organizing operations, including removal of the censored data, outlier correction, and data distribution analysis.

Various geophysical methods are used to explore deposits. Magnetometry is the most common geophysical method used in both airborne and surface methods. According to the local scale of the exploration, 4446 surface points were measured through the magnetometer operation on a 20×50 network. Through the processing of the magnetometry signal over the NPCD, alteration mapping can be deduced.

In mineral exploration, remote sensing is often used to distinguish hydrothermal alteration zones, faults, and lineaments (Honarmand et al., 2012; Mohammadpour et al., 2019). Satellite imagery with high spectral resolution (ASTER and Hyperspectral sensors) is used to define alteration zones (Fakhari et al., 2019; Honarmand et al., 2012), and high-resolution images such as panchromatic images are used to determine faults and lineaments in the image (Ahmadfaraj et al., 2019; Mohammadpour et al., 2019). In this study, the field survey results were used to determine the alteration according to the local scale, but the Quickbird image was used to determine the linear structures. The Quickbird satellite is capable of spatial resolutions of 0.61 m and 2.44 m with Pan and MS sensors, respectively, and it is currently among the most powerful commercial satellites in terms of ground resolution. Panchromatic band image with a spatial resolution of 0.61 m, developed in 2006, is used in this study.

At this stage of the study, drilling results are used to validate the mineral potential map. Within the studied area, 40 exploratory boreholes were drilled to evaluate the mining prospectivity of the NPCD.

4.2. Exploratory Target Criteria

Exploratory target criteria should be determined and defined based on the conceptual model of a mineralization system. There are many examples of mineral system models that cover different types of mineral resources and geological areas. Many models of existing mineral systems are very complex, incomplete, or contradictory because they are usually designed for a specific area, and each author presents

a model in a slightly different format. As such, existing mineral systems models are not easily usable in the EIS or are not applicable for targeting on a global scale. As a result, it is essential to continuously update and improve existing models (Yousefi et al., 2019). Since the studied deposit is of porphyry copper type, the mineralization and exploration characteristics of this type of deposit are presented here. Porphyry copper deposits include scattered copper ores and their variants in veins and incisions that are uniformly distributed in large amounts of rock and form high tonnages (more than 100 million tons) and have copper with the grades of 0.3-2%. Geological and geochemical evidence suggests that the porphyry copper systems are predominantly formed by thermal fluids released during the shallow replacement of porphyry granite stocks (John et al., 2010).

Porphyry copper deposits have been formed in most historical periods, but because unstable tectonic regions of bordering convergent plates are formed typically at the top of the crust (less than 5-10 km deep) and are vulnerable to erosion, more than 90% of known deposits are related to Cenozoic and Mesozoic in terms of the age (John et al., 2010).

Wide ranges of igneous rocks with different compounds are locally associated with and host the porphyry copper deposits. Quartz monzonite, diorite, granodiorite, dacite, andesite, quartz diorite, and monzonite are the most common types of reported rocks. Post-mineralization faults are also important in exploration and evaluation, in addition to their major role in maintaining porphyry copper deposits(John et al., 2010).

The major copper ores in the hypogenic ore are chalcopyrite and pyrite, which are found in almost all the deposits, and bornite, which is found in approximately 75% of the deposits. Molybdenite is the only major mineral in molybdenum, accounting for about 70% of the world's deposits. Au and Ag accounted for about 30% of deposits as an accompanying product or by-product and they are thought to be present in the bornite and chalcopyrite minerals. Rhenium is also obtained as a by-product of molybdenite. Supergene ore contains copper-extractable minerals and a large number of other minerals formed by the following: descending and groundwater with low pH that dissolves the hypogenic copper minerals and regenerates Cu in the stable minerals of the oxidative environments and low temperatures. The spatial distribution of Cu, Mo, Ag and Au is normally determined in Cu + / - Mo +/- Au porphyry mines for grade control and mining planning. The abundance of these and other sub-elements in rocks, soils, and sediments have been commonly used in the exploration of porphyry copper deposits (John et al., 2010).

The vary nature of porphyry copper system evolution concentrates minerals of diverse geophysical properties near the topographic surface. The distribution of magnetite in a porphyry copper deposit varies from abundant to insignificant, depending on the type and intensity of the alteration and parent lithology. The first stage of the alteration, along with porphyry copper deposits, occurs in areas that provide predictable spatial patterns of magnetic anomalies. A high-resolution surface magnetic investigation has been able to map these areas and provide useful exploration tools on a deposit scale (John et al., 2010).

In areas with good outcrops and limited vegetation, remote sensing by multi-spectral spatial imaging systems can be used to map transforming mineral complexes and their spatial relationships in porphyry copper systems. Minerals alterations such as phyllic (sericitic), argillic, propylitic, iron oxides, and silica can be mapped from a distance due to their special absorption properties in the visible spectrum to short-wave infrared and thermal infrared.

4.3. Target Proxies or Exploratory Layers

Criteria for the performance of mining subsystems, identified through the analysis of exploratory data, should be mapped as evidence of the document and/or proxy so that they can perform spatial analysis. It is important to note that some criteria may not be directly mapped, but maybe modeled as spatial proxies (Mccuaig et al., 2010). The characteristics of evidence and proxies are themselves indications of the rock formation processes that exist directly (i.e., the lithology extracted from the geological map) or indirectly (e.g., lithology interpreted from geophysical data) derived from the existing exploratory data set (Mccuaig et al., 2010). In this study, exploratory layers were produced using the criteria and characteristics of the deposit based on the available data and information.

4.3.1. Geology layers

I) Rock Types

Lithological and volcanic-volcanoclastic units with Eocene age and various phases of intrusive-subvolcanic units with Oligo-Miocene age are exposed in this region. The composition of volcanoclastic units is mainly medium to acidic tuffs and volcanic rocks include andesite and andesite basalt. All these units have been cut by Oligo-Miocene intrusive rocks, and they also account for the bulk of the outcrops in the area. The composition of intrusive rocks, including micro-quartz diorite, varies to granodiorite and dacite porphyry. The variety of sub-volcanic units in the area has been followed by successive replacing of intrusive stocks in earlier phases with very short time intervals, and a completely differentiated trend can also be observed in the intrusive rocks from the old to the new ones. The body of evidence is similar to the occurrence of a sub-volcanism associated with a Cu porphyry system. Finally, andesitic dikes have settled in the late stages of magmatism, which is a characteristic of porphyry Cu systems (Zarnab Co., 2011).

For integrating evidential layers, the rock types of the area were divided into nine classes and each class was assigned

an appropriate weight based on the conceptual model and expert knowledge. The rock types and the lithological evidential maps are shown in Figure 2.

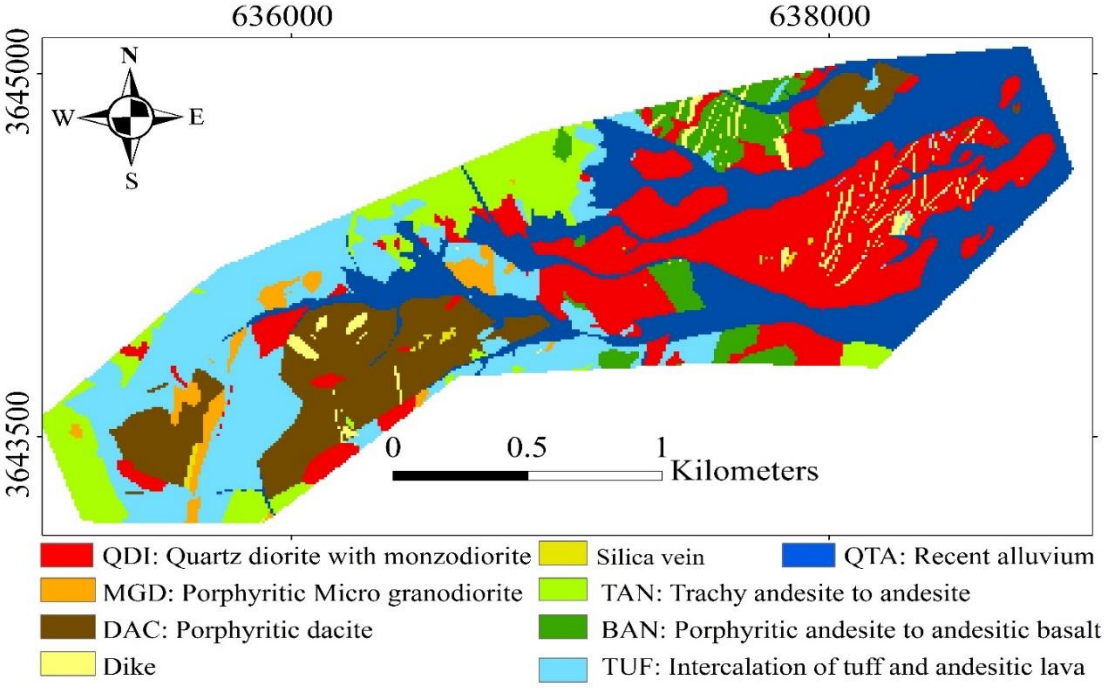

Figure 2. Rock type evidence map, based on 1: 5000 geological map.

II) Alteration

In this study, the alteration areas were determined by field survey according to the phase of exploration operations (Zarnab. Co, 2011). Thin section analysis, XRD, and surface geology in different parts of the NPCD proved that the most important alteration regions in Naysian were phyllic, potassic (biotite), propylitic (calcite, and chlorite), and Argillic, respectively. The most widespread alteration zone in the Naysian deposit is the phyllic alteration zone, which has affected many parts of the deposit with varying intensities. Most of the index minerals of the phyllic alteration present in the deposit are quartz, sericite, tourmaline, muscovite, pyrite, and anhydrite. Taking the results of the geological field survey into consideration, the regions with high mineralization rates are along with the phyllic zones. Therefore, the highest value was allocated to the phyllic alteration. A map of the alterations is shown in Figure 3.

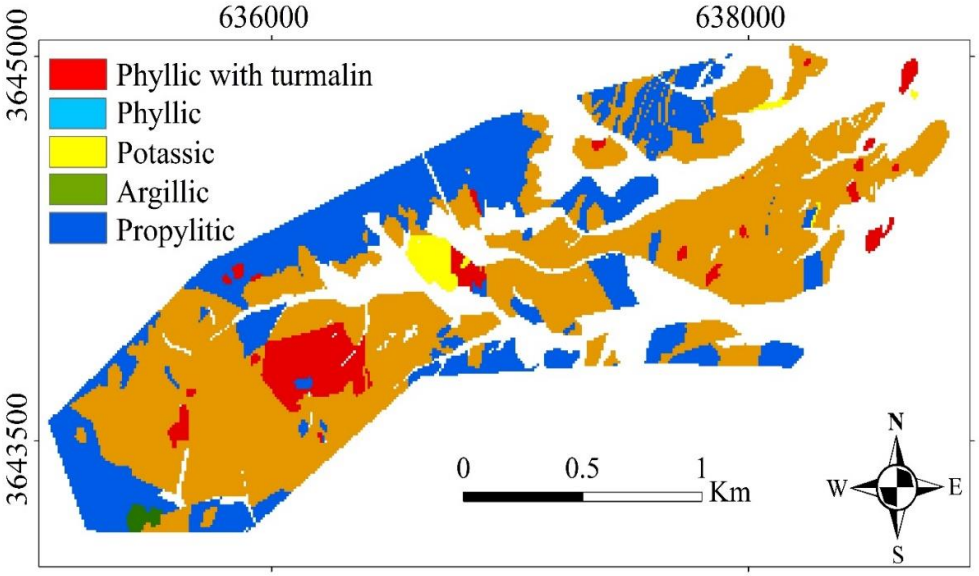

Figure 3 Alteration evidence map of the Naysian Porphyry copper district.

III) The density map of lineaments

It is an appropriate guide to identify the Cu mineralization place by determining the structural lineaments. Areas with tectonic evidence and high fault density are directly related

to mineralization (Ahmadfaraj et al., 2019). Lineaments were extracted from the 1:5000 geology map, the satellite images, and geomagnetic data, and finally, a density map was generated in this study., Fault traces derived from the field survey are shown in Figure 4a.

One powerful way to detect the lineaments on the ground surface is to use satellite images (Ahmadfaraj et al., 2019; Han et al., 2018; Mami Khalifani et al., 2019). Since the visual extraction of lineaments from the satellite images is the most common method, the automatic extraction techniques for detecting the lineaments can significantly reduce the user error and implementation time. The best automatic extraction techniques are those that integrate the edge detectors with the line extraction algorithms (Masoud & Koike, 2011; Rahnama & Gloaguen, 2014b). In the present study, Canny algorithm (Biswas & Sil, 2012) and Hough transform (Rahnama & Gloaguen, 2014a) were used as the edge detector filter and for extracting the linear features in an image, respectively.

These techniques were used on the images of the Quickbird satellite, which is capable of spatial resolution of 0.61 m and 2.44 m with Pan and MS sensors respectively. It is currently among the most powerful commercial satellites in terms of ground resolution. A panchromatic band image with a spatial resolution of 0.61 m, developed in 2006, is used in this study. The reason for such a selection is that it detects the several-ten-meter linear features as an important indicator layer in close association with the ore mineralization systems. After image corrections, the Canny filter is applied for detecting the edges in the line extraction phase, and then the Hough transform is used in the post-processing phase to enhance tectonic lineaments. The map of extracted lineaments related to the copper mineralization (Figure 4b) shows a prominent direction along the NE-SW.

Another way to detect the shallow and deep-seated lineaments is to use the geomagnetic data where they are called geophysical lineaments (Ajayakumar et al., 2017). The ground-based magnetometry survey was conducted over a 5.2 km^2 area with a grid of 20×50 m, where 4446 data were measured with a proton magnetometer. After diurnal correction, the regional magnetic effect was removed from the observations. There are many techniques to determine the geomagnetic lineaments, most of which are based on the directional derivatives of the potential field magnetometry data. The tilt angle method, relying on the initial concepts of the horizontal and vertical derivatives of the total field data (Miller & Singh, 1994), was used in this research. Before implementing the tilt angle filter, the reduced-to-pole (RTP) filter was applied on the residual magnetometry data to amplify the signal and correct the effect of the Earth's magnetic field inclination by putting the positive portion of anomalies over the main causative source(s) (Abedi and Oskooi, 2015). Figure 4c shows the output of the tilt angle method on the RTP data in the NPCD, where zero values locate over the shallow or deep-seated lineaments.

The final lineament map is generated by merging those derived from the geology map (field survey), Quickbird image, and the magnetometry data (Figure 4d). The generation of a lineament indicator map requires the classification of the lineament density using the fractal geometry concept that usually works well (Saein and Afzal, 2017; Yousefi and Carranza, 2015).

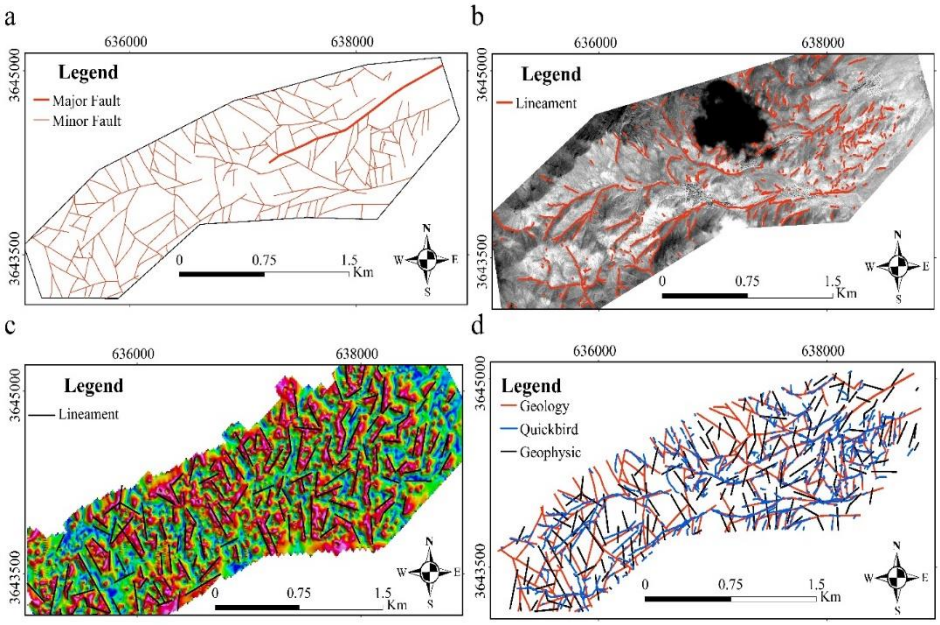

Figure 4 The structural lineaments in the Naysian region extracted from (a) field survey, (b) Quickbird satellite image processing, and (c) the tilt angle mapping of the ground-based magnetometry survey. (d) The final lineament map was generated by the integration of all ones.

To implement the C-A fractal method on the lineaments density map, values of lineaments density intensity were taken into account instead of the concentration values. On the basis of the diagram shown in Figure 5a, the fractal curve

was divided into four classes to obtain the fault density map (Figure 5b).

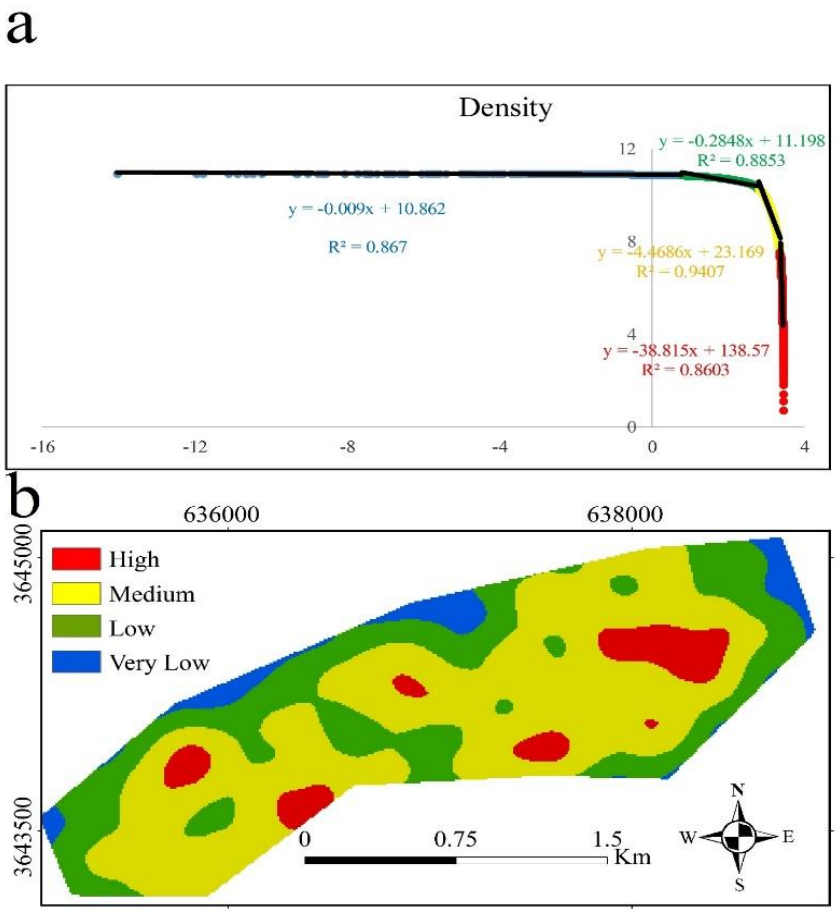

Figure 5 Evidence map of lineaments' density, a) C-A fractal curve for lineament density, and b) reclassified lineament density map based on the C-A fractal model.

4.3.2. Geochemical Layers

According to the conceptual model of porphyry copper deposits mentioned above, the spatial distribution of Cu, Mo, Au, and Ag is important for the exploration of porphyry copper deposits in geochemical methods. Bivariate and multivariate statistical analyses were performed on the data and the paragenesis of Cu and Mo was obtained from the results. Therefore, Cu and Mo were considered as the main evidential layers. The results of the soil geochemical data are in good agreement with the geological maps. Due to the characteristics of the ore deposit in the area and multivariate analysis of the geochemical layers of Cu, Mo, and factor 4 were selected as exploration layers.

I) Cu and Mo concentration maps

The resulting data from chemical analysis of the soil geochemical samples were arranged and after correction of the censored and outliers, the data were prepared for plotting of Cu and Mo geochemical maps. Then, geochemical maps of Cu and Mo were prepared using IDW interpolation method (Shepard, 1968). The anomaly from the background was separated using the C-A multifractal method as well.

The C-A fractal method was performed on geochemical maps and finally, the Cu and Mo maps were classified into four classes according to Figures 6a and 7a. Figures 6b and 7b present the geochemical maps of Cu and Mo, respectively. Most of the weight is assigned to areas with Cu and Mo anomalies, and more weight is assigned to the Cu evidence map due to the close association of Cu with mineralization.

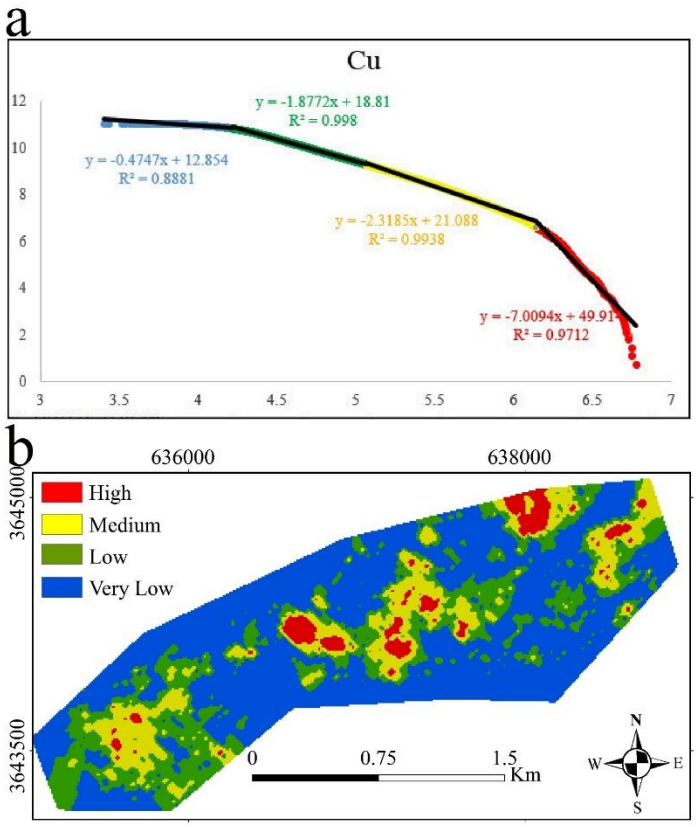

Figure 6 Geochemical evidence map of Cu, a) C-A fractal diagram for Cu, and b) reclassified geochemical map of Cu based on the C-A fractal model.

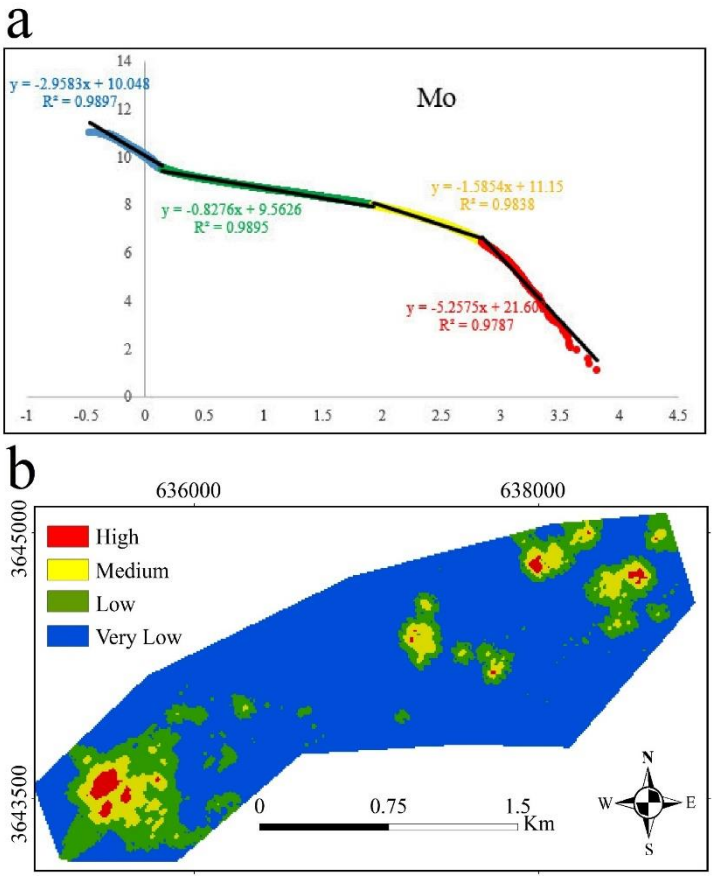

Figure 7 Geochemical evidence map of Mo, a) C-A fractal diagram for Mo, and b) reclassified geochemical map of Mo based on the C-A fractal model.

II) Factor Analysis

Multivariate statistical methods are widely used in the investigation of the elemental geochemical patterns by coping with simultaneous changes of several variables and their statistical inferences. They are used more than the univariate or bivariate statistical techniques in geoscience studies (Howarth, 1983) such that they can be utilized for searching the geochemical anomalies (Aliyari et al., 2020; Loska & Wiechuła, 2003). The factor analysis used here is among the valid and important multivariate methods. The number of the main initial variables is decreased by detecting the lengths with the most changes, and it is possible to investigate and identify the structures among the data. Therefore, both single- and multi-element variables can be analyzed to introduce the potential mineralized zones (Kumru & Bakaç, 2003). Through applying the factor analysis on the normalized values of variables (Table 1), the fourth factor with higher loading of Cu and Mo is selected as the main factor in association with the anomalous regions. According to Table 1, the Cu-Mo anomaly regions in factor 4 are shown with high values. Therefore, the C-A multifractal curve (Figure 8a) was plotted to generate the factor map. The high values of Factor 4, shown in red in Figure 8b, may indicate areas of Cu-Mo anomaly.

Table 1. Factor analysis table of the geochemical data.

Element	Factor 1	Factor 2	Factor 3	Factor 4	Factor 5	Factor 6
Ag	-0.008	-0.477	-0.155	0.172	0.401	-0.089
As	0.303	0.332	-0.459	-0.294	0.370	-0.298
Co	0.702	0.489	0.073	0.128	0.159	-0.190
Cr	0.634	-0.463	0.372	-0.105	0.041	-0.080
Cu	0.044	0.068	-0.099	0.415	0.091	0.390
Fe	0.639	0.241	0.163	0.223	0.186	0.013
Mn	0.678	0.120	-0.429	0.154	-0.130	-0.121
Mo	-0.321	0.243	0.137	0.353	0.220	0.122
Ni	0.671	-0.254	0.264	-0.380	0.075	0.083
P	0.179	-0.139	0.110	0.743	0.154	0.112
Pb	0.269	-0.064	-0.663	0.053	0.190	-0.160
S	-0.415	-0.126	0.066	0.280	0.582	-0.130
Sb	0.125	0.112	-0.586	-0.311	0.236	0.302
Sn	0.080	-0.756	0.138	0.189	0.055	0.073
Ti	0.680	0.179	-0.029	-0.015	-0.326	-0.162
V	0.838	-0.237	0.084	0.192	-0.110	-0.006
W	0.142	0.036	-0.573	0.318	0.283	0.386
Zn	0.585	0.130	-0.572	-0.064	0.120	-0.124

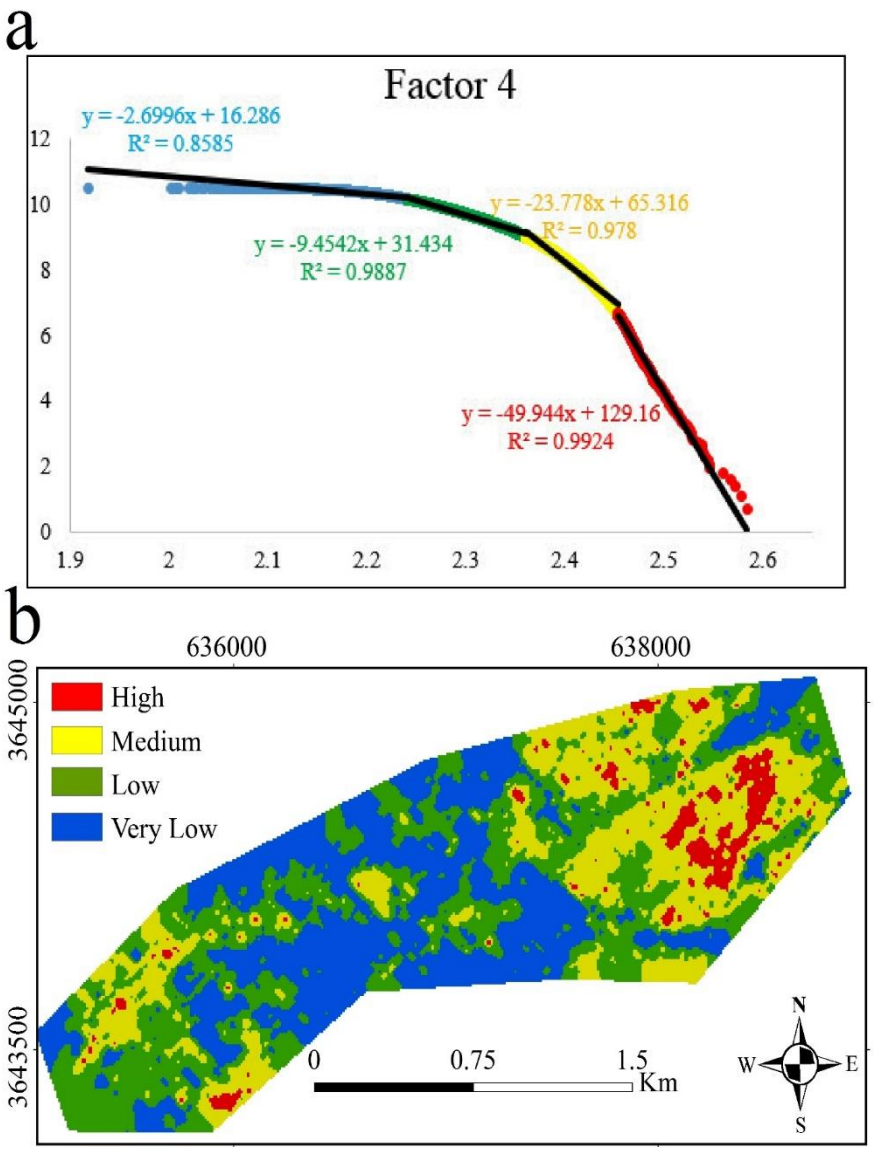

Figure 8 Geochemical evidence map of Factor 4, a) C-A fractal diagram for Factor 4, and b) reclassified geochemical map of Factor 4 based on the C-A fractal model.

4.3.3. Geophysical Layer

Simple models for porphyry copper deposits (Berger et al., 2008; Lowell & Guilbert, 1970) involve contrasting zones of alteration centered on the deposit. Magnetic anomalies can reflect the location of these zones: weak local magnetic highs over the potassic zone, low magnetic intensity over the sericitic zones, and gradually increasing intensities over the propylitic zone (Thoman et al., 1997). Therefore, areas with moderate magnetic intensity can be a sign of phyllic alteration in porphyry copper deposits. In the NPCD, since the phyllic alteration is expanding and mineralization is observed in this alteration, the moderate magnitude is given the highest weight.

Various techniques were proposed to enhance potential field magnetometry data that are the directional gradients, downward continuation, and several high-pass filters (Mami Khalifani et al., 2019; Shahsavar et al., 2019). One of these filters is the analytic signal (AS), which is advantageous to enhance the borders and the main body of sought targets. The initial formulation of the analytic signal filter for magnetic data was discussed by Nabighian (1974). This filter can better present the borders of the magmatic intrusive-related sources in the studied area. The analytic signal map was implemented on the RTP magnetometry data and then classified after applying the C-A multifractal method (Figure 9a). Since Cu-Mo mineralization occurred mostly on the margins of causative sources, those promising regions were closely related to the medium values of this filter. The geophysical map used in the integration model is shown in Figure 9b.

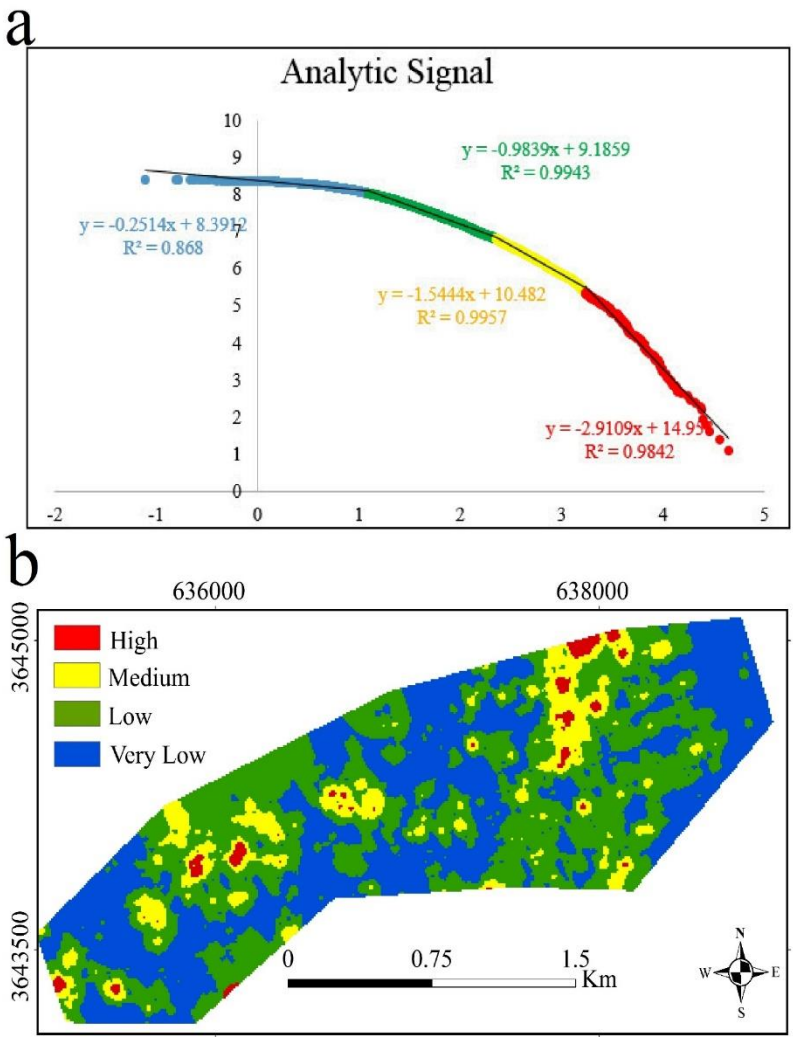

Figure 9. Geophysical evidence map of the magnetometry survey, (a) C-A fractal curve, and b) reclassified geophysics map based on the C-A fractal model.

4.4. **Geospatial Evidence Integration**

There is a consensus among geo-mathematical scientists that areas with higher statistical or conceptual characteristics (for example, higher weights) have a higher priority for subsequent explorations than those with lower ones (Yousefi & Carranza, 2016). Therefore, the best integration function is one that can use any of these features. Various integration functions have been developed and used to combine maps, i.e. weight exploration layers, and to generate exploratory targets. The effectiveness of the integration functions in the preparation of the mineral potential map has been used under the influence of the nature of data entry (for example, the quality of the forecast maps) and the applied weighted methods. Therefore, different integration functions should be considered to select the best and most suitable exploration targets. In this regard, three integration methods of the IO, C-VIKOR, and A-VIKOR have been evaluated here.

A geospatial decision matrix of 7×36791 was formed to integrate the seven layers prepared from geology, geophysics, and geochemistry. The decision tree shown in Figure 10 illustrates the inference network for the integration of layers. Mineral potential maps were obtained by three methods of the IO, C-VIKOR, and A-VIKOR. Assuming weights assigned to each layer presented in Table 2, the IO method was implemented as a popular and linear method of data integration for MPM. The integration result is plotted by the IO in Figure 11a, where higher values correspond to favorable regions with higher Cu mineralization desirability. Several zones are promising in the eastern, northeast, central, and western parts, depicted by red color in Figure 11a.

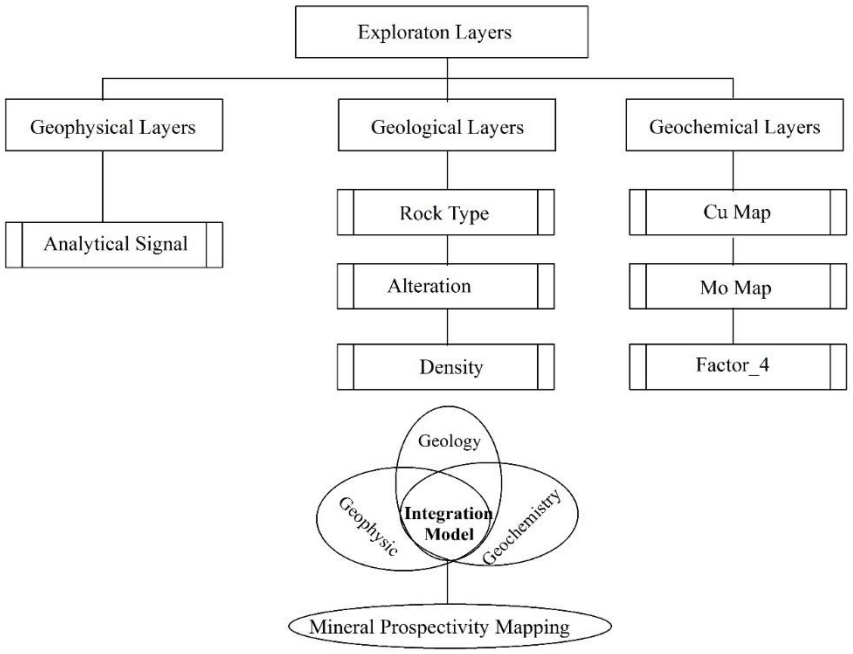

Figure 10. Flowchart of mineral potential mapping in the Naysian porphyry copper deposit.

Table 2: The normalized weight of each criterion acquired from a group of geoscientist decision-makers.

Criterion	Weight	Sub-criterion	Weight	Final weight
Geology	0.388	Lithology	0.332	0.1288
		Alteration	0.345	0.1339
		Density	0.323	0.1253
Geochemistry	0.499	Cu	0.425	0.2121
		Mo	0.270	0.1347
		Factor	0.305	0.1522
Geophysics	0.113	AS	1	0.113

The VIKOR approach is among the most widely used MCDM methods that are able to systematically prioritize the available options according to the criteria. Due to the high capability of this method, various researchers have used this approach to model MCDM problems (Opricovic & Tzeng, 2004). The reasons for the wide use of this method to prioritize options are (a) the logic used in the VIKOR method is understandable, (b) the computational processes are simple, (c) it provides the best consensus solution, and (d) this method provides, at the same time, proximity to the maximum mineral potential and the maximum distance from the region of sterility or background in the calculations in simple mathematical form.

In this research, the C-VIKOR and A-VIKOR methods were used for MPM. Regarding the implementation stages of the C-VIKOR and A-VIKOR methods in Section 2.1, these methods were applied to obtain the mineral potential maps according to Figures 11b and 11c, respectively.

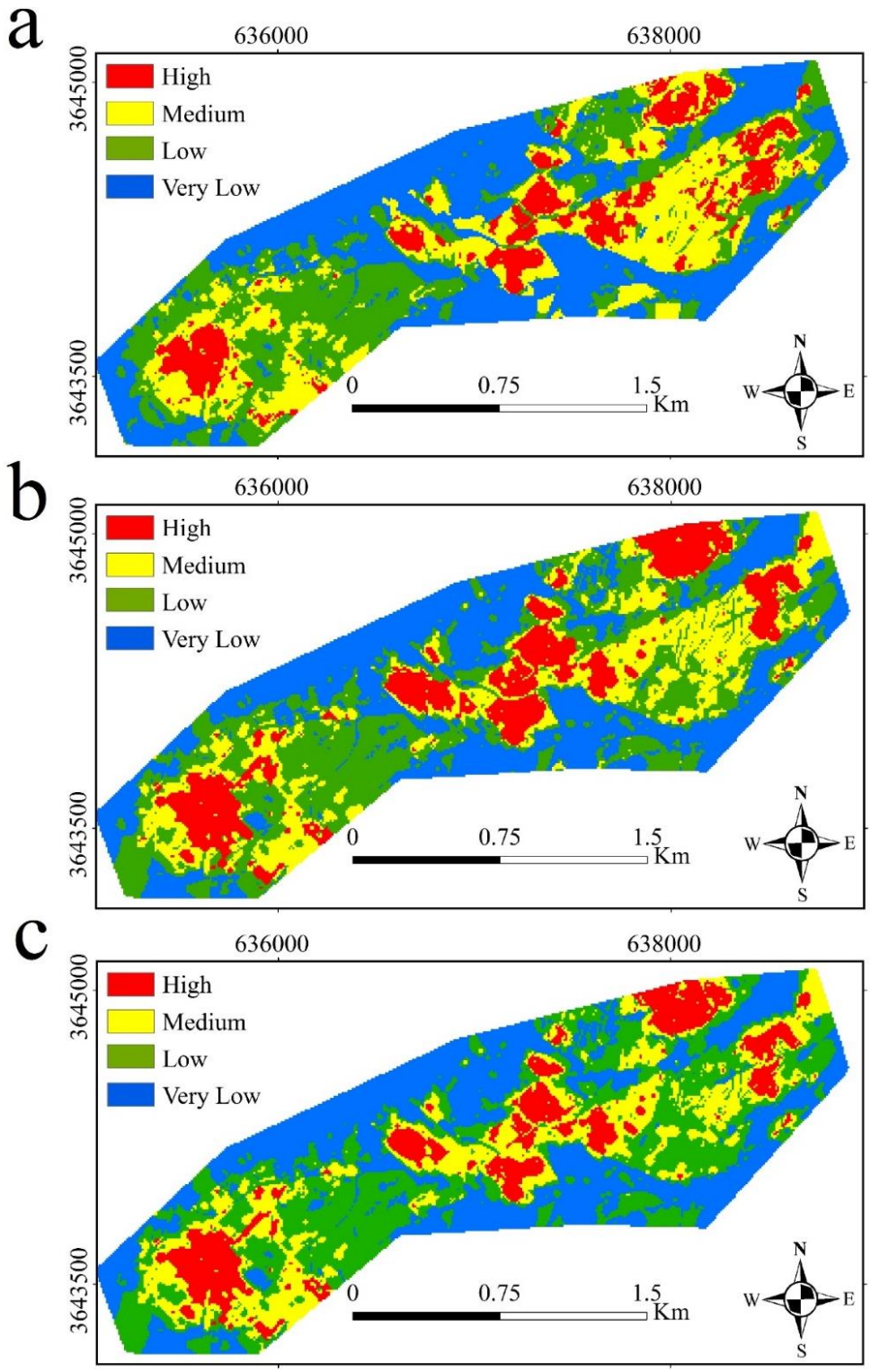

Figure 11 MPM derived from three algorithms of a) IO method, b) A-VIKOR method, and c) C-VIKOR method.

5. Discussion

Within the studied area, 40 exploratory boreholes were drilled to evaluate the mining prospectivity of the NPCD. The Cu concentration analysis was also made using an atomic absorption system. To validate the results obtained from this study, the average copper concentration in each borehole is calculated via Eq. (13):

$$\overline{Cu} = \frac{\sum_{i=1}^{n} Cu_i * T_i}{\sum_{i=1}^{n} T_i} \quad (13)$$

where Cu_i is the copper concentration in i^{th} sample, T_i is the borehole thickness of i^{th} sample, and n is the number of samples in each borehole.

Once the copper concentration was calculated in each borehole, its value was compared to those of MPM

(independent outputs) generated by the three aforementioned strategies. In Figure 12, the horizontal axis shows the average copper concentration and the orthogonal one indicates the MPM value in the pixel of borehole locations. The Top, middle, and lower rows in Figure 12 are derived from the IO, A-VIKOR, and C-VIKOR strategies, respectively. Higher Cu concentrations must correlate with the higher values in generated MPMs. Therefore, as the fitted line slope (between the MPM versus the Cu concentration) is closer to a line with a slope of $\alpha = 45^0$, it indicates the greater accuracy of MPM. As seen in Figure 12, positive slopes of all fitted lines indicate the efficiency of the VIKOR technique in MPM generation, where those related to the A-VIKOR method are more than the IO and C-VIKOR methods. As this value is 36^0 for the A-VIKOR map, it led to higher accuracy of the MPM. A notable point is that a positive correlation (or slope) exists between the A-VIKOR map and Cu concentrations, demonstrating more favorable regions in association with higher potential of Cu mineralization.

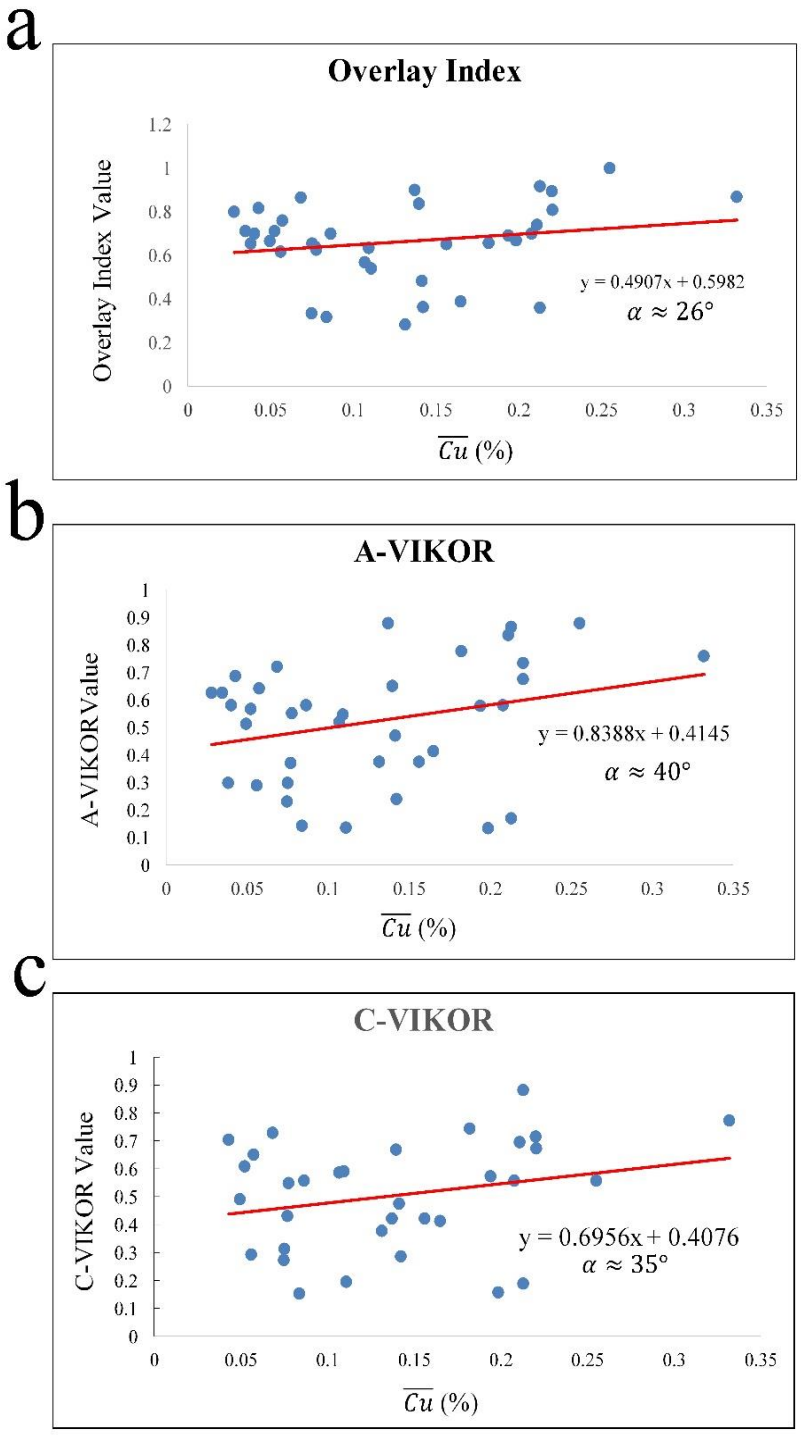

Figure 12 Scatter plot of the average copper concertation versus the value of MPM, a) IO method, b) A-VIKOR, and c) C-VIKOR.

In preparing a synthesized geospatial map, a method is preferred that introduces less area as prospectivity areas because it will reduce exploration costs in later stages. In addition, the success rate of the method can be taken into consideration through drilled boreholes in the region. An average copper grade above 0.1% was observed in 25 out of 40 drilled boreholes, Therefore, these 25 boreholes were considered as the criteria of measurement. In the MPM binary map by the IO method (Figure 13 a), 20 boreholes (80%) are located within prospectivity areas with an area of 0.495 Km^2. In the MPM binary map by the A-VIKOR method (Figure 13b), 23 boreholes (92%) are located in the prospectivity section with an area of 0.158 km^2. In addition to covering a larger number of boreholes, this map also introduces a smaller area than the IO method, implying that the A-VIKOR method is superior to the IO method. In the MPM by the C-VIKOR method (Figure13 c), 23 boreholes (92%) are located in the prospectivity section with an area of 0.187 km^2. Therefore, it has introduced more boreholes than the IO method and more area than the A-VIKOR method. In this study, the A-VIKOR method is superior to C-VIKOR and IO methods and there is a higher probability of success and deposit discovery.

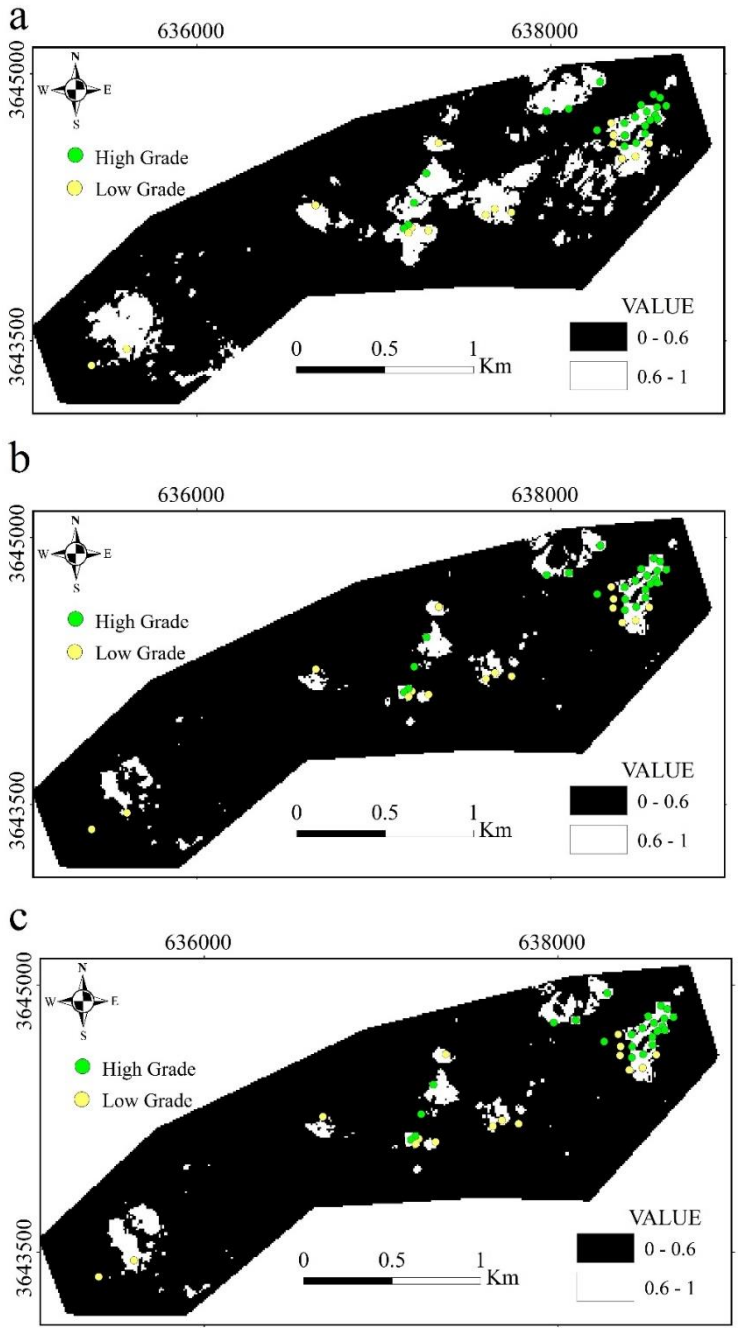

Figure 13 The binary mineral prospectivity mapping, a) IO method, b) A-VIKOR, and c) C-VIKOR.

6. Conclusion

The VIKOR method is one of the MCDM methods used for MPM. Based on consensus planning, this method evaluates issues with inappropriate and incompatible criteria and is effective in deciding on mineral potential issues. In this study, geochemical, geological, and geophysical evidential maps were prepared based on a porphyry copper deposit in the Naysian district. The highest weight was assigned to the geochemical layer of Cu and the lowest weight to the geophysical layer due to the mineralization potential of porphyry copper. MPM was prepared using the IO, A-VIKOR, and C-VIKOR methods. In these maps, high values are associated with promising areas of Cu mineralization. With a threshold of 0.6 for the maps obtained from the three methods, the area of promising zones are 49.5, 15.8, and 18.7 hectares for IO, A-VIKOR, and C-VIKOR methods, respectively. Therefore, the VIKOR methods introduce less area as promising areas, which reduces the risk of exploration. A comparison of the results obtained from exploratory boreholes between the three proposed methods reveals that the A-VIKOR method has higher accuracy and provides better results. Therefore, high-value areas in the A-VIKOR mineral potential map are suggested for drilling and further mining prospectivity.

Acknowledgment

The authors appreciate the Iranian National Copper Industry Company for handing over the data, information, and reports on the Naysian copper mineral district. We thank our colleagues from the School of Mining Engineering, University of Tehran who provided insight and expertise that greatly assisted the research.

References

Abedi, M., Ali Torabi, S., Norouzi, G. H., Hamzeh, M., & Elyasi, G. R. (2012). PROMETHEE II: A knowledge-driven method for copper exploration. *Computers and Geosciences*, *46*, 255–263. https://doi.org/10.1016/j.cageo.2011.12.012

Abedi, M., Mohammadi, R., Norouzi, G. H., & Mohammadi, M. S. M. (2016). A comprehensive VIKOR method for integration of various exploratory data in mineral potential mapping. *Arabian Journal of Geosciences*, *9*(6). https://doi.org/10.1007/s12517-016-2512-9

Abedi, M., & Norouzi, G. H. (2016). A general framework of TOPSIS method for integration of airborne geophysics, satellite imagery, geochemical and geological data. *International Journal of Applied Earth Observation and Geoinformation*, *46*, 31–44. https://doi.org/10.1016/j.jag.2015.11.016

Abedi, M., Norouzi, G. H., & Bahroudi, A. (2012). Support vector machine for multi-classification of mineral prospectivity areas. *Computers and Geosciences*, *46*, 272–283. https://doi.org/10.1016/j.cageo.2011.12.014

Abedi, M., Norouzi, G. H., & Fathianpour, N. (2012). Fuzzy outranking approach: A knowledge-driven method for mineral prospectivity mapping. *International Journal of Applied Earth Observation and Geoinformation*, *21*(1), 556–567. https://doi.org/10.1016/j.jag.2012.07.012

Abedi, M., Torabi, S. A., & Norouzi, G. H. (2013). Application of fuzzy AHP method to integrate geophysical data in a prospect scale, a case study: Seridune copper deposit. *Bollettino Di Geofisica Teorica Ed Applicata*, *54*(2), 145–164. https://doi.org/10.4430/bgta0085

Afshooni, S. Z., Mirnejad, H., Esmaeily, D., & Asadi Haroni, H. A. (2013). Mineral chemistry of hydrothermal biotite from the Kahang porphyry copper deposit (NE Isfahan), Central Province of Iran. *Ore Geology Reviews*, *54*, 214–232. https://doi.org/10.1016/j.oregeorev.2013.04.004

Afzal, P., Ahari, H. D., Omran, N. R., & Aliyari, F. (2013). Delineation of gold mineralized zones using concentration–volume fractal model in Qolqoleh gold deposit, NW Iran. *Ore Geology Reviews*, *55*, 125–133. https://doi.org/10.1016/j.oregeorev.2013.05.005

Afzal, P., Harati, H., Fadakar Alghalandis, Y., & Yasrebi, A. B. (2013). Application of spectrum-area fractal model to identify of geochemical anomalies based on soil data in Kahang porphyry-type Cu deposit, Iran. *Chemie Der Erde - Geochemistry*, *73*(4), 533–543. https://doi.org/10.1016/j.chemer.2013.08.001

Afzal, P., Khakzad, A., Moarefvand, P., Omran, N. R., Esfandiari, B., & Fadakar, Y. (2010). Geochemical anomaly separation by multifractal modeling in Kahang (Gor Gor) porphyry system , Central Iran. *Journal of Geochemical Exploration*, *104*(1–2), 34–46. https://doi.org/10.1016/j.gexplo.2009.11.003

Aghanabati, A. (2004). *Geology of Iran*. Geological Survey of Iran publication (In Persian).

Ahmadfaraj, M., Mirmohammadi, M., Afzal, P., Yasrebi, A. B., & Carranza, E. J. (2019). Fractal modeling and fry analysis of the relationship between structures and Cu mineralization in Saveh region, Central Iran. *Ore Geology Reviews*, *107*(January), 172–185. https://doi.org/10.1016/j.oregeorev.2019.01.026

Ajayakumar, P., Rajendran, S., & Mahadevan, T. M. (2017). Geophysical lineaments of Western Ghats and adjoining coastal areas of central Kerala, southern India and their temporal development. *Geoscience Frontiers*, *8*(5), 1089–1104. https://doi.org/10.1016/j.gsf.2016.11.005

Alavi, M. (2004). Regional Stratigraphy of the Zagros Fold-Thrust Belt of Iran and Its Proforeland Evolution. *American Journal of Science*, *304*, 1–20. http://dx.doi.org/10.2475/ajs.304.1.1%0A%0A

Aliyari, F., Afzal, P., Lotfi, M., Shokri, S., & Feizi, H. (2020). Delineation of geochemical haloes using the developed zonality index model by multivariate and fractal analysis in the Cu–Mo porphyry deposits. *Applied Geochemistry*, *121*(June), 104694. https://doi.org/10.1016/j.apgeochem.2020.104694

Asadi Haroni, H. A. (2007). *Detailed exploration in Kahang porphyry Cu-Mo index*.

Azadi, M., Mirmohammadi, M., & Hezarkhani, A. (2015). Aspects of magmatic–hydrothermal evolution of Kahang porphyry copper deposit, Central Iran. *Arabian Journal of Geosciences*, *8*(7), 4873–4893. https://doi.org/10.1007/s12517-014-1528-2

Berberian, F., & Berberian, M. (1981). *Tectono-plutonic episodes in Iran* (pp. 5–32). American Geophysical Union. https://doi.org/10.1029/GD003p0005

Berger, B. R., Ayuso, R. A., Wynn, J. C., & Seal, R. R. (2008). *Preliminary Model of Porphyry Copper Deposits: U.S. Geological Survey Open-File Report*. U.S. Geological Survey.

Billa, M., Stein, G., Guillou-Frottier, L., Tourlière, B., Bouchot, V., Lips, A. L. ., & Cassard, D. (2004). Predicting gold-rich epithermal and porphyry systems in the central Andes with a continental-scale metallogenic GIS. *Ore Geology Reviews*, *25*(1–2), 39–67. https://doi.org/10.1016/j.oregeorev.2004.01.002

Biswas, R., & Sil, J. (2012). An Improved Canny Edge Detection Algorithm Based on Type-2 Fuzzy Sets. *Procedia Technology*, *4*, 820–824. https://doi.org/10.1016/j.protcy.2012.05.134

Bonham-Carter, G. F. (1994). *Geographic Information Systems for Geoscientists Modelling with GIS* (1st ed.). Pergamon. https://doi.org/https://doi.org/10.1016/C2013-0-03864-9

Cargill, S. M., & Clark, A. L. (1978). Report on the activity of IGCP Project 98. *Journal of the International Association for Mathematical Geology*, *10*(5), 411–417. https://doi.org/10.1007/BF02461973

Carranza, E. J M, van Ruitenbeek, F. J. A., Hecker, C., van der Meijde, M., & van der Meer, F. D. (2008). Knowledge-guided data-driven evidential belief modeling of mineral prospectivity in Cabo de Gata, SE Spain. *International Journal of Applied Earth Observation and Geoinformation*, *10*(3), 374–387. https://doi.org/10.1016/j.jag.2008.02.008

Carranza, Emmanuel John M. (2009). *Geochemical anomaly and mineral prospectivity mapping in GIS*. Elsevier.

Carranza, Emmanuel John M. (2010). Improved wildcat modelling of mineral prospectivity. *Resource Geology*, *60*(2), 129–149. https://doi.org/10.1111/j.1751-3928.2010.00121.x

Carranza, Emmanuel John M., & Laborte, A. G. (2015). Random forest predictive modeling of mineral prospectivity with small number of prospects and data with missing values in Abra (Philippines). *Computers and Geosciences*, *74*, 60–70. https://doi.org/10.1016/j.cageo.2014.10.004

Cheng, Q., Agterberg, F. P., & Ballantyne, S. B. (1994). The separation of geochemical anomalies from background by fractal methods. *Journal of Geochemical Exploration*, *51*(2), 109–130. https://doi.org/10.1016/0375-6742(94)90013-2

Fakhari, S., Jafarirad, A., Afzal, P., & Lotfi, M. (2019). Delineation of hydrothermal alteration zones for porphyry systems utilizing ASTER data in Jebal-Barez area, SE Iran. *Iranian Journal of Earth Sciences*, *11*(1), 80–92.

Farmahini Farahani, M. (2008). *Geology, geochemistry and mineralogy investigations of Kahang index*. Islamic Azad University Science and Research Branch, Tehran, Iran.

Ghezelbash, R., & Maghsoudi, A. (2018). A hybrid AHP-VIKOR approach for prospectivity modeling of porphyry Cu deposits in the Varzaghan District, NW Iran. *Arabian Journal of Geosciences*, *11*(11). https://doi.org/10.1007/s12517-018-3624-1

Han, L., Liu, Z., Ning, Y., & Zhao, Z. (2018). Extraction and analysis of geological lineaments combining a DEM and remote sensing images from the northern Baoji loess area. *Advances in Space Research*, *62*(9), 2480–2493. https://doi.org/10.1016/j.asr.2018.07.030

Hatami, S. (2008). *Petrology of Kahang granitoids and volcanic rocks with emphasis on mineralization and alteration zones*. Islamic Azad University Khorasgan Branch, Isfahan, Iran.

Honarmand, M., Ranjbar, H., & Shahabpour, J. (2012). Application of Principal Component Analysis and Spectral Angle Mapper in the Mapping of Hydrothermal Alteration in the Jebal-Barez Area, Southeastern Iran. *Resource Geology*, *62*(2), 119–139. https://doi.org/10.1111/j.1751-3928.2012.00184.x

Hosseini, M. (2011). *geological and alteration studies of Kahang district, scale: 1:1000*.

Howarth, R. J. (1983). *Statistics and Data Analysis in Geochemical Prospecting* (1st Editio). Elsevier Science.

Jahan, A., Mustapha, F., Ismail, M. Y., Sapuan, S. M., & Bahraminasab, M. (2011). A comprehensive VIKOR method for material selection. *Materials and Design*, *32*(3), 1215–1221. https://doi.org/10.1016/j.matdes.2010.10.015

John, D. A., Ayuso, R. A., Barton, M. D., Blakely, R. J., Bodnar, R. J., Dilles, J. H., Graybeal, F. T., Mars, J. C., McPhee, D. K., Seal, R. R., & others. (2010). Porphyry copper deposit model. *Scientific Investigations Report*, 169.

Kumru, M. N., & Bakaç, M. (2003). R-mode factor analysis applied to the distribution of elements in soils from the Aydin basin, Turkey. *Journal of Geochemical Exploration*, *77*(2–3), 81–91. https://doi.org/10.1016/S0375-6742(02)00271-6

Laudon, K. C., & Laudon, J. P. (2014). *Management Information Systems: Managing The digital Firm* (13th ed.). Pearson Education.

Loska, K., & Wiechuła, D. (2003). Application of principal component analysis for the estimation of source of heavy metal contamination in surface sediments from the Rybnik Reservoir. *Chemosphere*, *51*(8), 723–733. https://doi.org/10.1016/S0045-6535(03)00187-5

Lowell, j. D., & Guilbert, J. M. (1970). Lateral and Vertical Alteration-Mineralization Zoning in Porphyry Ore Deposits. *Economic Geology*, *65*, 373–408.

Luo, X., & Dimitrakopoulos, R. (2003). Data-driven fuzzy analysis in quantitative mineral resource assessment. *Computers and Geosciences*, *29*(1), 3–13. https://doi.org/10.1016/S0098-3004(02)00078-X

Mami Khalifani, F., Bahroudi, A., Aliyari, F., Abedi, M., Yousefi, M., & Mohammadpour, M. (2019). Generation of an efficient structural evidence layer for

mineral exploration targeting. *Journal of African Earth Sciences*, *160*(103609), 1–20. https://doi.org/10.1016/j.jafrearsci.2019.103609

Mandelbrot, B. B. (1983). *The Fractal Geometry of Nature* (updated an). Freeman.

Masoud, A. A., & Koike, K. (2011). Auto-detection and integration of tectonically significant lineaments from SRTM DEM and remotely-sensed geophysical data. *ISPRS Journal of Photogrammetry and Remote Sensing*, *66*(6), 818–832. https://doi.org/10.1016/j.isprsjprs.2011.08.003

Mccuaig, T. C., Beresford, S., & Hronsky, J. (2010). Translating the mineral systems approach into an effective exploration targeting system. *Ore Geology Reviews*, *38*(3), 128–138. https://doi.org/10.1016/j.oregeorev.2010.05.008

Miller, H. G., & Singh, V. (1994). Potential field tilt a new concept for location of potential field sources. *Journal of Applied Geophysics Volume 32*, *32*(2–3), 213–217.

Mohammadpour, M., Bahroudi, A., Abedi, M., Rahimipour, G., Jozanikohan, G., & Khalifani, F. M. (2019). Geochemical distribution mapping by combining number-size multifractal model and multiple indicator kriging. *Journal of Geochemical Exploration*, *200*. https://doi.org/10.1016/j.gexplo.2019.01.018

Mohammadpour, Mahyadin, Alahveisi, K., & Bahroudi, A. (2019). *Automatic lineament extraction from ASTER images using the Hough transform , JabalBarez 1 : 100000 sheet*. *9*(4), 374–391. https://doi.org/10.22055/aag.2019.25774.1850

Najafi, A., Karimpour, M. H., & Ghaderi, M. (2014). Application of fuzzy AHP method to IOCG prospectivity mapping: A case study in Taherabad prospecting area, eastern Iran. *International Journal of Applied Earth Observation and Geoinformation*, *33*(1), 142–154. https://doi.org/10.1016/j.jag.2014.05.003

Oh, H. J., & Lee, S. (2010). Application of artificial neural network for gold-silver deposits potential mapping: A case study of Korea. *Natural Resources Research*, *19*(2), 103–124. https://doi.org/10.1007/s11053-010-9112-2

Opricovic, S. (1998). *Multicriteria Optimization of Civil Engineering Systems*. Belgrade.

Opricovic, S., & Tzeng, G. H. (2004). Compromise solution by MCDM methods: A comparative analysis of VIKOR and TOPSIS. *European Journal of Operational Research*, *156*(2), 445–455. https://doi.org/10.1016/S0377-2217(03)00020-1

Porwal, A., Carranza, E. J. M., & Hale, M. (2001). Extended weights-of-evidence modelling for predictive mapping of base metal deposit potential in Aravalli Province, western India. *Exploration and Mining Geology*, *10*(4), 273–287. https://doi.org/10.2113/0100273

Porwal, A., Carranza, E. J. M., & Hale, M. (2003). Artificial neural networks for mineral-potential mapping: A case study from Aravalli Province, Western India. *Natural Resources Research*, *12*(3), 155–171. https://doi.org/10.1023/A:1025171803637

Porwal, A., Carranza, E. J. M., & Hale, M. (2006). A hybrid fuzzy weights-of-evidence model for mineral potential mapping. *Natural Resources Research*, *15*(1), 1–14. https://doi.org/10.1007/s11053-006-9012-7

Rahnama, M., & Gloaguen, R. (2014a). TecLines: A MATLAB-based toolbox for tectonic lineament analysis from satellite images and DEMs, part 2: Line segments linking and merging. *Remote Sensing*, *6*(11), 11468–11493. https://doi.org/10.3390/rs61111468

Rahnama, M., & Gloaguen, R. (2014b). TecLines: A MATLAB-Based Toolbox for Tectonic Lineament Analysis from Satellite Images and DEMs, Part 1: Line Segment Detection and Extraction. *Remote Sensing*, *6*(7), 5938–5958. https://doi.org/10.3390/rs6075938

Sabahi, F., Lotfi, M., Afzal, P., & Nezafati, N. (2019). Geological, fluid inclusion and isotopic characteristics of the Gardaneshir Zn-Pb deposit, Central Iran. *Geopersia*, *9*(2), 221–232. https://doi.org/10.22059/GEOPE.2019.268248.648421

Saein, L. D., & Afzal, P. (2017). Correlation between Mo mineralization and faults using geostatistical and fractal modeling in porphyry deposits of Kerman Magmatic Belt, SE Iran. *Journal of Geochemical Exploration*, *181*(September 2016), 333–343. https://doi.org/10.1016/j.gexplo.2017.06.014

Shahsavar, S., Jafari Rad, A., Afzal, P., Nezafati, N., & Akhavan Aghdam, M. (2019). Prospecting for polymetallic mineralization using step-wise weight assessment ratio analysis (SWARA) and fractal modeling in Aghkand Area, NW Iran. *Arabian Journal of Geosciences*, *12*(7). https://doi.org/10.1007/s12517-019-4304-5

Shepard, D. (1968). A two-dimensional interpolation for irregularly-spaced data function. *Proceedings of the 1968 ACM National Conference*, 517–524. https://doi.org/10.1145/800186.810616

Stocklin, J. (1968). Structural History and Tectonics of Iran: A Review. In *American Association of Petroleum Geologists. AAPG Bulletin* (Vol. 52, Issue 7). American Association of Petroleum Geologists. http://archives.datapages.com/data/bulletns/1968-70/data/pg/0052/0007/1200/1229.htm

Tabatabaei, S.H., Asadi Haroni, H. (2006). Geochemical characteristics of Gor GorCu–Mo porphyry system. *25th Iranian Symposium on Geosciences*, 60.

Tavana, M., & Hatami-Marbini, A. (2011). A group AHP-TOPSIS framework for human spaceflight mission planning at NASA. *Expert Systems with Applications*, *38*(11), 13588–13603. https://doi.org/10.1016/j.eswa.2011.04.108

Thoman, M. W., Geologist, R., & Phelps, M. (1997). *GEOPHYSICAL CASE HISTORY OF NORTH SILVER BELL , PIMA CO ., ARIZONA : A SUPERGENE-ENRICHED PORPHYRY COPPER DEPOSIT*. Spokane, Washington, Northwest Mining Associationfile:///E:/Lesson/Doctora/lesson/Thesis/Paper/Integration/VIKOR/Revise1/paper/lowell1970.pdf.

Yousefi, M., & Carranza, E. J. M. (2015). Prediction-area (P-A) plot and C-A fractal analysis to classify and evaluate evidential maps for mineral prospectivity modeling. *Computers and Geosciences*, *79*, 69–81.

https://doi.org/10.1016/j.cageo.2015.03.007

Yousefi, M., & Carranza, E. J. M. (2016). Data-Driven Index Overlay and Boolean Logic Mineral Prospectivity Modeling in Greenfields Exploration. *Natural Resources Research*, *25*(1), 3–18. https://doi.org/10.1007/s11053-014-9261-9

Yousefi, M., Kreuzer, O. P., Nykänen, V., & Hronsky, J. M. A. (2019). Exploration information systems – A proposal for the future use of GIS in mineral exploration targeting. *Ore Geology Reviews*, *111*(July). https://doi.org/10.1016/j.oregeorev.2019.103005

Zarnab.Co. (2011). *Geological and alteration studies of Kahang area*.

Zuo, R., Agterberg, F. P., Cheng, Q., & Yao, L. (2009). Fractal characterization of the spatial distribution of geological point processes. *International Journal of Applied Earth Observation and Geoinformation*, *11*(6), 394–402. https://doi.org/10.1016/j.jag.2009.07.001